Simulation and Optimal Control of Molten Carbonate Fuel Cells

K. Chudej, K. Sternberg, H.J. Pesch, Universität Bayreuth, Germany

Corresponding Author: K. Chudej
Universität Bayreuth, Lehrstuhl für Ingenieurmathematik
Universitätsstr. 30, 95440 Bayreuth, Germany
e-mail: kurt.chudej@uni-bayreuth.de

Abstract. Molten carbonate fuel cells (MCFC) are especially well suited for stationary power plants if their process heat is used to increase their efficiency. MCFCs seem to become soon competitive compared with traditional power plants. The dynamic behavior of MCFCs can be modelled mathematically by a hierarchy of systems of quasi linear partial differential algebraic equations in 1D or 2D. Integral terms appear and the nonlinear boundary conditions are given partly by a DAE system. These large PDAE systems of dimension up to 28 equations are discretized by the method of lines, yielding huge dimensional DAEs. A short overview of an index analysis is given. Numerical simulation results for a 2D dynamical model including a detailed modelling of the reactions in the pores are presented as well as new numerical results for a (sub)optimal control during load changes of the power plant.

Keywords. PDE constrained optimal control, PDAE, fuel cell, time index.

1. 2D Dynamic Model of a Molten Carbonate Fuel Cell

Molten carbonate fuel cells (MCFCs) are especially well suited for stationary power plants if their process heat is used to increase their efficiency. MCFCs seem to become soon competitive compared to traditional power plants. In order to enhance service life, high temperature gradients inside the fuel cells must be avoided. Therefore control strategies are currently under development. Admittedly, not only the avoidance of high temperature gradients is of interest, but also the optimization of the efficiency of fuel cell systems.

The dynamic behavior of MCFCs can be modeled mathematically by a hierarchy of systems of partial differential algebraic equations; see Heidebrecht and Sundmacher [7, 8] and, in particular, Heidebrecht [6]. A detailed description of a certain 1D model together with an index analysis concerning the (differential) time and spatial indices as well as the MOL index and some numerical results can be found in Chudej et al. [4].

The 2D model investigated in the present paper describes an MCFC with a cross flow mode for the guidance of the anode and cathode gas streams. Such a design has been realized for the so-called *HotModule* produced by the MTU CFC Solutions GmbH, Munich, and is operated among others by the IPF-Heizkraftwerksbetriebsgesellschaft mbH, Magdeburg, at the power plant of the University Hospital of Magdeburg. See Fig. 1 for a schematic picture of the main devices of the Hot Module, which has been taken into account in the mathematical model. The anode inlet, at which the feed gas is fed in, is on the south-west side of the fuel cell. The anode outlet gas is directed into the cathode inlet on the south-east side of the fuel cell via a catalytic combustor and reversal chamber. The exhaust gas at the cathode outlet finally goes to the cell exhaust device.

In the anode and cathode gas channels, resp., the following chemical reactions take place. Within the gas stream of the anode channel an internal reforming can be performed due to the high operating temperature to produce the necessary hydrogen:

$$\begin{array}{lcllcll} \mathrm{CH_4} & + & \mathrm{H_2O} & \rightleftharpoons & \mathrm{CO} & + & 3\,\mathrm{H_2}\,, \\ \mathrm{CO} & + & \mathrm{H_2O} & \rightleftharpoons & \mathrm{CO_2} & + & \mathrm{H_2}\,. \end{array} \tag{1}$$

Simultaneously, an electro-chemical reaction, the oxidation reaction, takes place at the anode electrode:

$$\begin{array}{lcllcll} \mathrm{H_2} & + & \mathrm{CO_3^{2-}} & \rightleftharpoons & \mathrm{H_2O} + \mathrm{CO_2} & + & 2\mathrm{e^-}\,, \\ \mathrm{CO} & + & \mathrm{CO_3^{2-}} & \rightleftharpoons & 2\,\mathrm{CO_2} & + & 2\mathrm{e^-}\,. \end{array} \tag{2}$$

In contrast, at the cathode electrode we have the reduction reaction:

$$\frac{1}{2}\mathrm{O_2} + \mathrm{CO_2} + 2\mathrm{e^-} \rightleftharpoons \mathrm{CO_3^{2-}}\,. \tag{3}$$

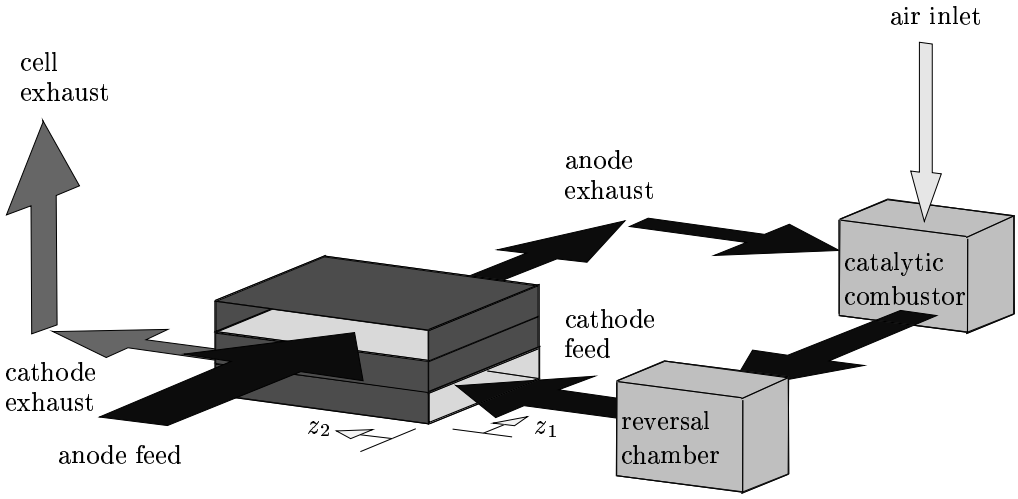

Figure 1: 2D cross flow configuration of the Hot Module

Hereby, the carbonate ions produced in the cathode channel are transferred through the electrolyte from the cathode electrode to the anode electrode. Bipolar plates serve as heat conducting material and separate the single cells of the stack. From the cell's outside, the electric current can be collected at the electrodes; see Fig. 2. For the sake of simplicity, we use here a 1D figure for a cell with a counter flow configuration in order to describe the gas flows and the dominating chemical reactions. The model however treats the cross flow configuration and the chemical reactions (1–3).

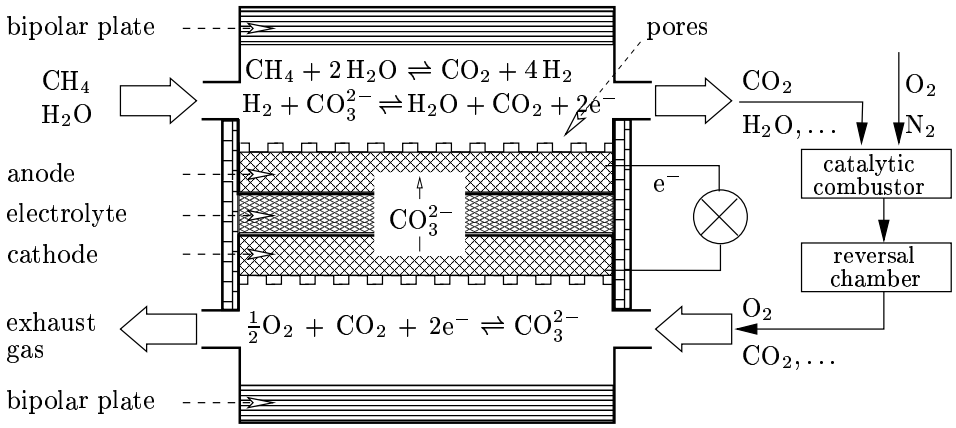

Figure 2: 1D counterflow model describing gas flow and simplified chemical reactions

In the anode and cathode channels 7 substances arise in the chemical reactions: methane CH_4, hydrogen H_2, water H_2O, oxygen O_2, carbon monoxide CO, carbon dioxide CO_2, and nitrogen N_2. The molar fractions of all these substances in the gas flows of the two channels are denoted by $\chi_{a,j}$ and $\chi_{c,j}$, $j = 1, \ldots, 7$, resp. The molar fractions in the pores of the electrodes are denoted by $p_{a,j}$ and $p_{c,j}$. For the numerical treatment we have to include only four variables $p_{a,j}$ associated with H_2O, H_2, CO, CO_2 in the pores of the anode and two variables $p_{c,j}$ associated with CO, CO_2 in the pores of the cathode. Further, we have to take into account the molar flow densities γ_a and γ_c as well as the temperatures θ_a and θ_c in the anode and cathode gas channels. These temperatures θ_a and θ_c are dominated by convection and are to be distinguished from the solid temperature θ_s, which is distributed through the solid by diffusion, i.e. heat conduction. Moreover, the electrical potentials Φ_a^L, Φ_c^L, and Φ_c^S at which anode ion layer, cathode ion layer and cathode electrode are relative to a reference potential, and the current density i are introduced into the model. The total cell current $I_{cell} = I_{cell}(t)$ is usually prescribed.

Altogether, we end up with a system of time t dependent nonlinear partial differential algebraic equations in two space dimensions $z := (z_1, z_2) \in \Omega := [0,1]^2$ corresponding to the two gas flow directions due to the cross flow configuration of the stack. The large scale coupled model developed in [6] consists of the following parts:

Heat equation in the solid:

$$\frac{\partial \theta_\mathrm{s}}{\partial t} = \lambda\, \Delta\theta_\mathrm{s} + \varphi_1(\theta_\mathrm{s}, \theta_\mathrm{a}, \theta_\mathrm{c}, \chi_\mathrm{a}, \chi_\mathrm{c}, p_\mathrm{a}, p_\mathrm{c}, \Phi_\mathrm{a}^\mathrm{L}, \Phi_\mathrm{c}^\mathrm{L}, \Phi_\mathrm{c}^\mathrm{S})\,, \qquad \lambda \text{ positive constant.} \tag{4}$$

Advection equations in the gas streams:

$$\frac{\partial \chi_{\mathrm{a},j}}{\partial t} = -\gamma_\mathrm{a}\theta_\mathrm{a}\,\frac{\partial \chi_{\mathrm{a},j}}{\partial z_1} + \varphi_{2,j}(\theta_\mathrm{s}, \theta_\mathrm{a}, \chi_\mathrm{a}, p_\mathrm{a}, \Phi_\mathrm{a}^\mathrm{L})\,, \qquad j = 1, \ldots, 7\,, \tag{5}$$

$$\frac{\partial \chi_{\mathrm{c},j}}{\partial t} = -\gamma_\mathrm{c}\theta_\mathrm{c}\,\frac{\partial \chi_{\mathrm{c},j}}{\partial z_2} + \varphi_{3,j}(\theta_\mathrm{s}, \theta_\mathrm{c}, \chi_\mathrm{c}, p_\mathrm{c}, \Phi_\mathrm{c}^\mathrm{L}, \Phi_\mathrm{c}^\mathrm{S})\,, \qquad j = 1, \ldots, 7\,, \tag{6}$$

$$\frac{\partial \theta_\mathrm{a}}{\partial t} = -\gamma_\mathrm{a}\theta_\mathrm{a}\,\frac{\partial \theta_\mathrm{a}}{\partial z_1} + \varphi_4(\theta_\mathrm{s}, \theta_\mathrm{a}, \chi_\mathrm{a}, p_\mathrm{a}, \Phi_\mathrm{a}^\mathrm{L})\,, \tag{7}$$

$$\frac{\partial \theta_\mathrm{c}}{\partial t} = -\gamma_\mathrm{c}\theta_\mathrm{c}\,\frac{\partial \theta_\mathrm{c}}{\partial z_2} + \varphi_5(\theta_\mathrm{s}, \theta_\mathrm{c}, \chi_\mathrm{c}, p_\mathrm{c}, \Phi_\mathrm{c}^\mathrm{L}, \Phi_\mathrm{c}^\mathrm{S})\,. \tag{8}$$

Degenerated PDEs for the molar flows:

$$0 = \frac{\partial(\gamma_\mathrm{a}\theta_\mathrm{a})}{\partial z_1} + \varphi_8(\theta_\mathrm{s}, \theta_\mathrm{a}, \chi_\mathrm{a}, p_\mathrm{a}, \Phi_\mathrm{a}^\mathrm{L})\,, \qquad 0 = \frac{\partial(\gamma_\mathrm{c}\theta_\mathrm{c})}{\partial z_2} + \varphi_9(\theta_\mathrm{s}, \theta_\mathrm{c}, \chi_\mathrm{c}, p_\mathrm{c}, \Phi_\mathrm{c}^\mathrm{L}, \Phi_\mathrm{c}^\mathrm{S})\,. \tag{9}$$

Algebraic equations in the pores:

$$p_{\mathrm{a},j} = \varphi_{6,j}(p_\mathrm{a}, \theta_\mathrm{s}, \chi_\mathrm{a}, \Phi_\mathrm{a}^\mathrm{L})\,,\ j = 1, \ldots, 4, \qquad p_{\mathrm{c},j} = \varphi_{7,j}(p_\mathrm{c}, \theta_\mathrm{s}, \chi_\mathrm{c}, \Phi_\mathrm{c}^\mathrm{L}, \Phi_\mathrm{c}^\mathrm{S})\,,\ j = 1, 2. \tag{10}$$

Integro PDAE system for the potentials:

$$\frac{\partial \Phi_\mathrm{a}^\mathrm{L}}{\partial t} = [i_\mathrm{a}(p_\mathrm{a}, \theta_\mathrm{s}, \Phi_\mathrm{a}^\mathrm{L}) - i]/c_\mathrm{a}\,, \qquad c_\mathrm{a}, c_\mathrm{c} \text{ constants,} \tag{11}$$

$$\frac{\partial \Phi_\mathrm{c}^\mathrm{L}}{\partial t} = [i_\mathrm{a}(p_\mathrm{a}, \theta_\mathrm{s}, \Phi_\mathrm{a}^\mathrm{L}) - i]/c_\mathrm{a} + [i_\mathrm{e}(\Phi_\mathrm{a}^\mathrm{L}, \Phi_\mathrm{c}^\mathrm{L}) - i]/c_\mathrm{c}\,, \tag{12}$$

$$\frac{\mathrm{d}\Phi_\mathrm{c}^\mathrm{S}}{\mathrm{d}t} = \varphi_{10}\left(\int_\Omega i_\mathrm{a}(p_\mathrm{a}, \theta_\mathrm{s}, \Phi_\mathrm{a}^\mathrm{L})\,\mathrm{d}z, \int_\Omega i_\mathrm{c}(p_\mathrm{c}, \theta_\mathrm{s}, \Phi_\mathrm{c}^\mathrm{L}, \Phi_\mathrm{c}^\mathrm{S})\,\mathrm{d}z, \int_\Omega i_\mathrm{e}(\Phi_\mathrm{a}^\mathrm{L}, \Phi_\mathrm{c}^\mathrm{L})\,\mathrm{d}z, I_\mathrm{cell}\right)\,. \tag{13}$$

where the current density $i = i(t, z)$ is given by

$$i = \varphi_{11}\left(i_\mathrm{a}, i_\mathrm{c}, i_\mathrm{e}, \int_\Omega i_\mathrm{a}\,\mathrm{d}z, \int_\Omega i_\mathrm{c}\,\mathrm{d}z, \int_\Omega i_\mathrm{e}\,\mathrm{d}z, I_\mathrm{cell}\right)$$

and the total cell current $I_\mathrm{cell}(t)$, which is given.

All functions determined by the quasi-linear PDAEs are functions of z and t except $\Phi_\mathrm{c}^\mathrm{S} = \Phi_\mathrm{c}^\mathrm{S}(t)$. The presentation of all smooth source terms φ_j, $j = 1, \ldots, 11$, as well as of the smooth functions i_a, i_c, and i_e in full detail would be beyond the scope of this paper; they can be found in Heidebrecht [6]. Summarizing we obtain a nonlinear PDAE system of dimension 28.

For simulations, the boundary conditions for the temperature θ_a, the molar fractions $\chi_{\mathrm{a},j}$ and the molar flow γ_a are prescribed at the anode inlet, i. e., at $z_1 = 0$, $z_2 \in [0,1]$ (usually only as time dependent functions), compare Fig. 1. For the temperature θ_c, the molar fractions $\chi_{\mathrm{c},j}$ and the molar flow γ_c the boundary conditions at the cathode inlet, i. e., at $z_2 = 0$, $z_1 \in [0,1]$, depend on the corresponding output values at the anode outlet, i. e., at $z_1 = 1$, $z_2 \in [0,1]$, and from the environment. These values are given via the solution of a system of ordinary differential algebraic equations. It describes the time dependent behavior of the gas temperature, the molar fractions and the molar flow in the catalytic combustor and the reversal chamber. Note that these quantities depend on the averaged values of the associated quantities

at the anode outlet. Again, without giving the details for the smooth right hand sides φ_j, $j = 12, \ldots, 14$, of the ordinary DAE system, the boundary conditions at the cathode inlet can be read as follows:

$$\chi_{\mathrm{c},j}(t,z)\Big|_{z_1\in[0,1],\, z_2=0} = \chi_{\mathrm{m},j}(t), \quad j = 1,\ldots,7\,, \tag{14}$$

$$\theta_{\mathrm{c}}(t,z)\Big|_{z_1\in[0,1],\, z_2=0} = \theta_{\mathrm{m}}(t)\,, \quad \gamma_{\mathrm{c}}(t,z)\Big|_{z_1\in[0,1],\, z_2=0} = \gamma_{\mathrm{m}}(t) \tag{15}$$

where

$$\frac{\mathrm{d}\chi_{\mathrm{m},j}}{\mathrm{d}t} = \varphi_{12,j}\left(\chi_{\mathrm{m}}, \theta_{\mathrm{m}}, \int_0^1 \chi_{\mathrm{a}}\Big|_{z_1=1}\mathrm{d}z_2, \int_0^1 \theta_{\mathrm{a}}\Big|_{z_1=1}\mathrm{d}z_2, \int_0^1 \gamma_{\mathrm{a}}\Big|_{z_1=1}\mathrm{d}z_2, \chi_{\mathrm{air}}, \lambda_{\mathrm{air}}\right)\,, \tag{16}$$

$$\frac{\mathrm{d}\theta_{\mathrm{m}}}{\mathrm{d}t} = \varphi_{13}\left(\theta_{\mathrm{m}}, \int_0^1 \chi_{\mathrm{a}}\Big|_{z_1=1}\mathrm{d}z_2, \int_0^1 \theta_{\mathrm{a}}\Big|_{z_1=1}\mathrm{d}z_2, \int_0^1 \gamma_{\mathrm{a}}\Big|_{z_1=1}\mathrm{d}z_2, \theta_{\mathrm{air}}, \chi_{\mathrm{air}}, \lambda_{\mathrm{air}}\right)\,, \tag{17}$$

$$\gamma_{\mathrm{m}} = \varphi_{14}\left(\theta_{\mathrm{m}}, \int_0^1 \chi_{\mathrm{a}}\Big|_{z_1=1}\mathrm{d}z_2, \int_0^1 \theta_{\mathrm{a}}\Big|_{z_1=1}\mathrm{d}z_2, \int_0^1 \gamma_{\mathrm{a}}\Big|_{z_1=1}\mathrm{d}z_2, \theta_{\mathrm{air}}, \chi_{\mathrm{air}}, \lambda_{\mathrm{air}}\right) \tag{18}$$

with initial conditions $\chi_{\mathrm{m},j}(0) = \chi_{\mathrm{m},j,0}$, $\theta_{\mathrm{m}}(0) = \theta_{\mathrm{m},0}$.

Here, θ_{air}, $\chi_{\mathrm{air},j}$, and λ_{air} denote the ambient temperature, the molar fractions of oxygen and nitrogen in air and the air number, resp. The latter defines the amount of air fed into the burner. All these quantities can be subject to changes in time and thus can play the roles of boundary controls.

Moreover, the boundary conditions for the solid temperature θ_{s} are, because of the insulation, given by zero Neumann conditions at the boundary of the electrolyte, i.e. at $\partial\Omega$. Finally, consistent initial conditions at time $t = 0$ for all $z \in \Omega$ must be suitably imposed, see Eq. (20).

2. Index Analysis of the PDAE

Index analysis of PDAEs is a young research topic. It started with the introduction of (DAE-)indices based on MOL-discretized or Laplace- or Fourier-transformed versions of the PDAE and matured with the definition of algebraic, differential and perturbation indices of the PDAE itself (e.g. [2, 11, 12, 3, 5, 13, 9, 15, 14]).

2.1 Differential Time Index

The described 2D MCFC PDAE model is a member of the following class of PDAEs of mixed parabolic and hyperbolic type:

Find $\mathbf{u}(t,z)$ with time $t \in J = [0,T]$ and spatial coordinate $z \in \Omega = [0,1]^d$, $d \in \{1,2,3\}$, s.t.

$$A\mathbf{u}_t = B\Delta\mathbf{u} + \sum_{j=1}^{d} C_j[\mathbf{u}]\,\mathbf{u}_{z_j} + \Psi(\mathbf{u},t,z) \tag{19}$$

(A, B constant matrices, C_j affine linear matrices in $\mathbf{u}$) and initial conditions

$$A\left[\mathbf{u}(0,z) - \mathbf{g}(z)\right] = 0 \tag{20}$$

and suitable nonlinear boundary conditions. We assume that the PDAE has a sufficiently smooth solution.

The following definition is a generalization of [10] and [4]:

Definition. *If the matrix A is regular, the (differential) time index is defined to be $\nu := 0$. Otherwise the (differential) time index ν is the smallest number of times, the PDAE must be differentiated with respect to time t in order to determine $\mathbf{u}_t$ as a continuous function of $t, z, \mathbf{u}$ and spatial partial derivatives of $\mathbf{u}$.*

We consider at first a slightly simplified 2D model of the MCFC. We neglect the molar fractions in the pores and assume the electrical potentials to be constant and apply a coordinate transformation $v = \gamma_{\mathrm{a}}\theta_{\mathrm{a}}$

and $\bar{v} = \gamma_c \theta_c$ (the same is done for the boundary conditions). Then the Eqs. (4–9) together with simpler linear boundary conditions can be written as:

Find functions $u(t,z)$ (temperature of the solid), $v(t,z) > 0$, $\bar{v}(t,z) > 0$ (temperature times molar flow density of the gas in the anode and cathode gas channel) and $w(t,z)$, $\bar{w}(t,z)$ (temperature and molar fractions of the gas in the anode and cathode gas channel) s.t. the PDAE (with positive constant λ) on $[0,T] \times [0,1]^2$

$$\begin{aligned} u_t &= \lambda \Delta u + \psi_1(u,w,v,\bar{w},\bar{v}), && (21)\\ w_t &= -v\, w_{z_1} + \psi_2(u,w,v), && (22)\\ 0 &= v_{z_1} + \psi_3(u,w), && (23)\\ \bar{w}_t &= -\bar{v}\, \bar{w}_{z_2} + \psi_4(u,\bar{w},\bar{v}), && (24)\\ 0 &= \bar{v}_{z_2} + \psi_5(u,\bar{w}), && (25) \end{aligned}$$

with initial conditions

$$u(0,z) = g_1(z),\ w(0,z) = g_2(z),\ \bar{w}(0,z) = g_4(z), \qquad (26)$$

and nonlinear boundary conditions

$$\begin{aligned} \frac{\partial u}{\partial n}|_{\partial\Omega} &= 0, \qquad w(t,0,z_2) = w_{\text{west}}(t), \qquad v(t,0,z_2) = v_{\text{west}}(t), && (27)\\ \bar{w}(t,z_1,0) &= \bar{w}_{\text{south}}(t) = \phi_1\left(\xi(t), \int_0^1 w(t,1,z_2)\,\mathrm{d}z_2, \int_0^1 v(t,1,z_2)\,\mathrm{d}z_2\right), && (28)\\ \bar{v}(t,z_1,0) &= \bar{v}_{\text{south}}(t) = \phi_2\left(\xi(t), \int_0^1 w(t,1,z_2)\,\mathrm{d}z_2, \int_0^1 v(t,1,z_2)\,\mathrm{d}z_2\right), && (29) \end{aligned}$$

with a given continuously differentiable function $\xi(t)$. We assume that all given functions ψ_i, g_i, w_{west}, v_{west} are continuous with respect to all arguments. We assume that the given functions ψ_3 and ψ_5 are continuously differentiable with respect to all arguments. We assume that the given function v_{west} is continuously differentiable with respect to t. The given function ϕ_1 is assumed to be continuous, the given function ϕ_2 to be continuously differentiable with respect to all arguments. Consistency of initial and boundary conditions is assumed, i.e. $g_2(0,z_2) = w_{\text{west}}(0)$ and $g_4(z_1,0) = \bar{w}_{\text{south}}(0)$.

Theorem 1. *The differential time index of the PDAE (21–29) is $\nu = 1$.*

Proof. Partial differentiation of Eq. (23) with respect to time yields

$$0 = v_{tz_1} + \frac{\partial \psi_3}{\partial u} u_t + \frac{\partial \psi_3}{\partial w} w_t. \qquad (30)$$

Plugging in the r.h.s. of Eqs. (21, 22) yields

$$\frac{\partial}{\partial z_1} v_t = \alpha(u,w,v,\bar{w},\bar{v},\Delta u, w_{z_1}). \qquad (31)$$

By a similar computation one gets

$$\frac{\partial}{\partial z_2} \bar{v}_t = \bar{\alpha}(u,w,v,\bar{w},\bar{v},\Delta u, \bar{w}_{z_2}). \qquad (32)$$

Due to the assumptions α and $\bar{\alpha}$ are continuous with respect to all arguments. Therefore

$$\begin{aligned} v_t(t,z) &= \frac{\partial}{\partial t} v_{\text{west}}(t) + \int_0^{z_1} \alpha(u,w,v,\bar{w},\bar{v},\Delta u, w_{z_1})|_{(t,\tilde{z}_1,z_2)}\,\mathrm{d}\tilde{z}_1, && (33)\\ \bar{v}_t(t,z) &= \left(\frac{\mathrm{d}\xi(t)}{\mathrm{d}t}, \int_0^1 -vw_{z_1} + \psi_2(u,w,v)|_{(t,1,z_2)}\,\mathrm{d}z_2, \int_0^1 v_t(t,1,z_2)\,\mathrm{d}z_2\right) \cdot && (34)\\ &\cdot \ \operatorname{grad} \phi_2\left(\xi(t), \int_0^1 w(t,1,z_2)\,\mathrm{d}z_2, \int_0^1 v(t,1,z_2)\,\mathrm{d}z_2\right) + \\ &+ \int_0^{z_2} \bar{\alpha}(u,w,v,\bar{w},\bar{v},\Delta u,\bar{w}_{z_2})|_{(t,z_1,\tilde{z}_2)}\,d\tilde{z}_2, \end{aligned}$$

yields time index $\nu = 1$.

Theorem 2. *We consider the PDAE (4–18) with initial conditions of type (20). If we assume that the functions* $\int_0^1 \chi_{a,j}(t,1,z_2)\,dz_2$, $\int_0^1 \theta_a(t,1,z_2)\,dz_2$, $\int_0^1 \gamma_a(t,1,z_2)\,dz_2$ *are continuously differentiable with respect to time and that* $\chi_{air}(t)$, $\theta_{air}(t)$, $\lambda_{air}(t)$ *are continuously differentiable then the differential time index is* $\nu = 1$.

Proof. Investigation of the functions $\varphi_{6,j}$, $\varphi_{7,j}$ yields that the Eqs. (10) for the molar fractions in the pores are of time index one, since $\frac{\partial \varphi_6}{\partial p_a} \neq I$ and $\frac{\partial \varphi_7}{\partial p_c} \neq I$. The Eqs. (11-13) for the potentials are obviously of time index zero, if the electrical density i is considered only as an auxiliary function. The solution of the Eqs. (14-18) can be written as a nonlinear boundary condition of type (28, 29). Under the above assumptions the functions $\xi(t) = (\chi_{air}(t), \theta_{air}(t), \lambda_{air}(t))$ and $\chi_m(t), \theta_m(t)$ are continuously differentiable, therefore ϕ_1 and ϕ_2 and all of their arguments are continuously differentiable. Application of Theorem 1 finishes the proof.

2.2 MOL Index

After an equidistant semi-discretization in space we get a semi-explicit differential algebraic initial value problem in time t for a huge dimensional variable $\mathbf{U}(t)$

$$\mathcal{A}\frac{d}{dt}\mathbf{U}(t) + b(\mathbf{U}(t), \Xi(t)) = 0, \qquad \mathcal{A}\,(\mathbf{U}(0) - \mathbf{U}_0) = 0. \tag{35}$$

The Laplace-Operator is approximated by the five-point-star. The first spatial partial derivatives are approximated by appropriate upwind formulas. The diagonal matrix $\mathcal{A}$ has zeros or ones in the diagonal.

$\mathbf{U}$ includes the component functions along the lines associated with the space discretization as well as the functions $\chi_m(t)$ and $\theta_m(t)$. $\Xi(t)$ denotes the boundary functions $w_{west}(t)$, $v_{west}(t)$ and $\chi_{air}(t)$, $\theta_{air}(t)$, $\lambda_{air}(t)$ which are either given or can be used for control purposes.

Theorem 3. *The MOL index of the semi-explicit DAEs derived from the previous PDAE models (21–29) and (4–18) is* $\nu_{MOL} = 1$.

The proof is based on the upwind formulas with known wind direction and the correctly posed boundary conditions of the PDAE, compare Chudej et al [4], Chap. 4.

A perturbation index of a semilinear version of the PDAE (21–26) with linear boundary conditions is computed in [15].

3. Numerical Simulation and Optimal Control

We have to solve an optimal control problem of the following type:

$$J[\tilde{\Xi}(\mathbf{t})] \to \min \quad \text{s.t.} \quad \text{PDAE with consistent initial and boundary conditions.} \tag{36}$$

In order to solve this complicated nonstandard optimal control problem we choose the approach to *first discretize, then optimize* in contrast to *first optimize, then discretize.* We favor this approach because of the various model updates in the past being typical when dealing with real world problems. This fact makes it (almost) impossible to apply the mathematically more safeguarded latter approach.

So, after an equidistant MOL discretization, we arrive at a huge dimensional standard optimal control problem of type

$$J[\tilde{\Xi}(\mathbf{t})] \to \min \quad \text{s.t.} \quad \text{DAE (35) with } \tilde{\Xi}(\mathbf{t}) \text{ a subset of } \Xi(t) \tag{37}$$

which can be handled by standard discretization approaches.

3.1 Numerical Simulation

In the following we present the numerical simulation results. The software package NUDOCCCS [1] developed for the numerical solution of large scale ODE and DAE constrained optimal control problems can be used for simulation purposes, too. The numerical integration of the DAE system is performed by a fifth order implicit Runge-Kutta method (RADAU 5).

The numerical solution of some selected components is depicted in the Figs. 3–10. The figures show the two-dimensional spatial distribution at a time, at which we assume that the steady state has been reached. About 10 000 time steps had to be performed. Further note that all quantities are dimensionless.

In each diagram, the inlet of the anode is on the south-west side ($z_1 = 0$, $z_2 \in [0,1]$), the cathode inlet is on the south-east side ($z_1 \in [0,1]$, $z_2 = 0$). The gas flows in z_1-direction through the anode channel, in z_2-direction through the cathode channel.

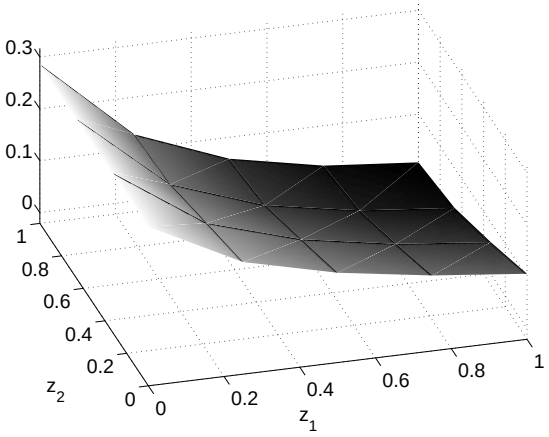

Figure 3: Methane $\chi_{\mathrm{a,CH_4}}$ [-] (anode channel)

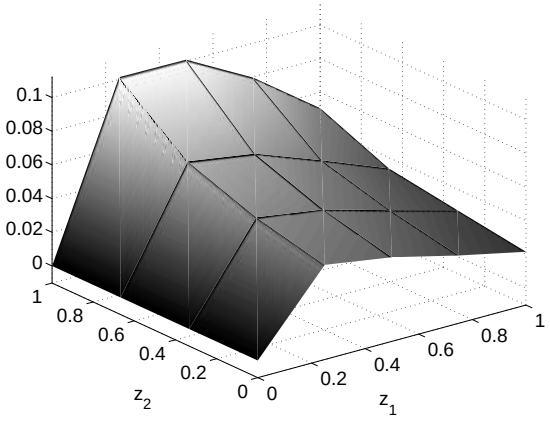

Figure 4: Hydrogen $\chi_{\mathrm{a,H_2}}$ [-] (anode channel)

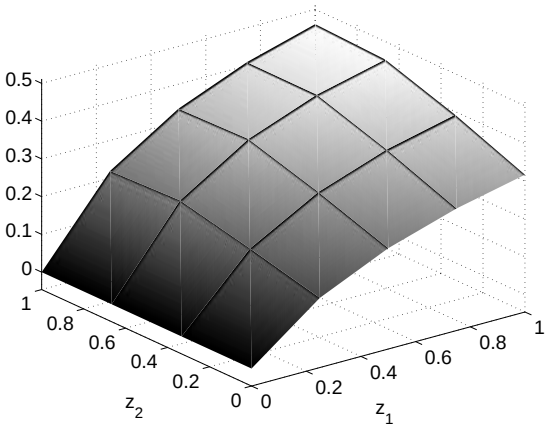

Figure 5: Carbon dioxide $\chi_{\mathrm{a,CO_2}}$ [-] (anode channel)

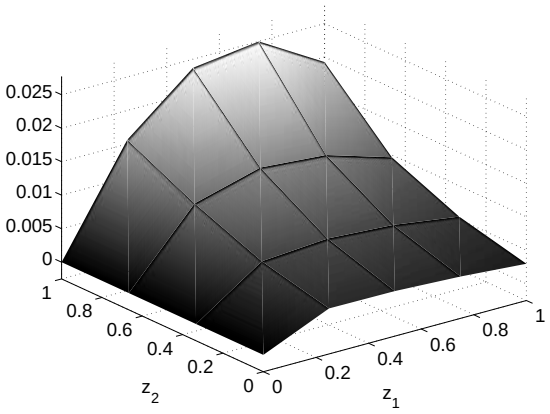

Figure 6: Carbon monoxide $\chi_{\mathrm{a,CO}}$ [-] (anode channel)

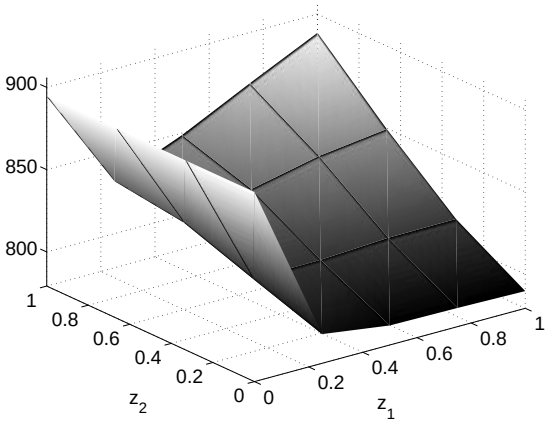

Figure 7: Temperature θ_{a} [K] (anode channel)

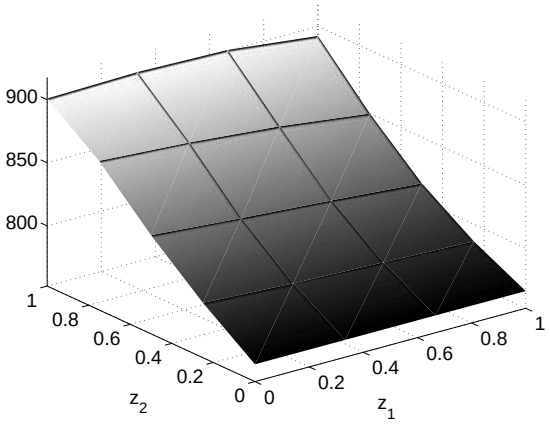

Figure 8: Temperature θ_{c} [K] (cathode channel)

The results obtained make sound sense as we will show. The methane depicted in Fig. 3 decreases over the entire width due to the methane consuming endothermic reforming reaction (1). The concentration is slightly lower on that side of the anode channel where the cathode outlet is located. This is due to the higher temperatures in this region leading to higher reforming reaction rates there.

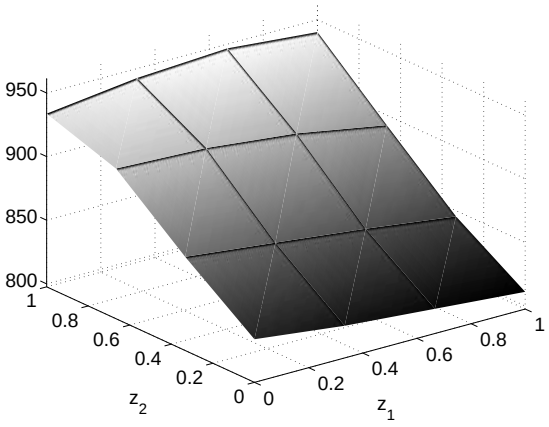

Figure 9: Temperature θ_s [K] (solid)

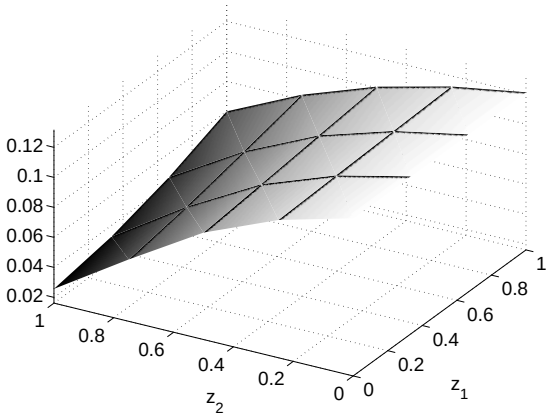

Figure 10: Carbon dioxide χ_{c,CO_2} [-] (cathode channel)

In accordance with the methane behavior hydrogen is produced in the endothermic reforming reaction (1) immediately after the anode inlet to be subsequently consumed in the exothermic oxidation reaction (2); see Fig. 4. Near $z_1 = 1$ and $z_2 = 1$, we see higher concentrations of hydrogen due to higher temperatures and consequently higher reforming reaction rates.

As can be seen from Fig. 10 the concentration of the carbon dioxide in the cathode decreases from the cathode inlet on the south-east side to its outlet on the north-west side due to the reduction reaction (3).

The most important results are concerned with the temperatures; see Figs. 7–9. They directly influence the reaction rates. Moreover, the solid temperature, see Fig. 9, must be particularly observed to avoid so-called hot spots leading to material corrosion and consequently to a reduced service life.

The temperature distribution in the anode channel coincides with the heat demand and the heat release of the reactions therein. Initially we have the endothermic reaction (1). Thus the temperature declines. In the following, the anode gas temperature is increased again by heat exchange with the solid, which is heated by the electro chemical reactions (2–3).

Since the solid temperature is not evenly distributed, see Fig. 9, the temperature in the anode channel has a local maximum near $z_1 = 1$ and $z_2 = 1$ due to heat conduction, see Fig. 7. The cathode gas is heated up by the solid phase all along the channel, so the temperature continuously increases along z_2, see Fig. 8.

3.2 Optimal Control of Load Changes

From a technical viewpoint optimal boundary control strategies for faster load changes of the fuel cell are of interest and are currently under development (Sternberg [16]). Fig. 11 depicts first results of a load change of the total cell current $I_{\text{cell}}(t)$ and a simulation result for the electric potential $\Phi_c^S(t)$ with prescribed $\lambda_{\text{air}}(t) \equiv 2.2$ and $\gamma_{\text{a,in}}(t) \equiv 1.0$ in Fig. 12. It is desirable to reach the new stationary value of the electric potential $\Phi_{c,\text{ref}}^S(t)$ earlier. This is formulated as an optimal control problem:

Find optimal time dependent boundary controls $\lambda_{\text{air}}(t) \in [2.1, 2.3]$ and $\gamma_{\text{a,in}}(t) \in [0.9, 1.1]$ in order to minimize a cost functional

$$\int_0^T \left[\Phi_c^S(t) - \Phi_{c,\text{ref}}^S(t)\right]^2 dt \tag{38}$$

s.t. to the DAE (35).

In order to cope with computing time and memory limitations instead a suboptimal control is computed by solving a sequence of optimal control problems on shorter time interval ls $[t_i, t_{i+1}]$, $i = 0, \ldots, M$,

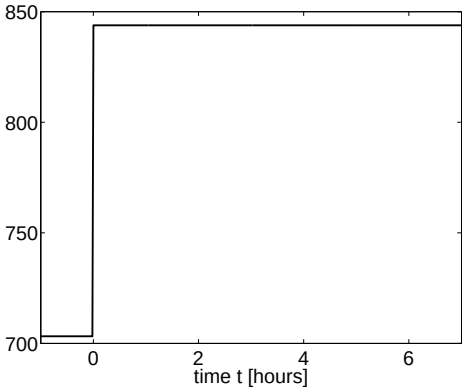

Figure 11: Load change of the total cell current I_{cell} [A]

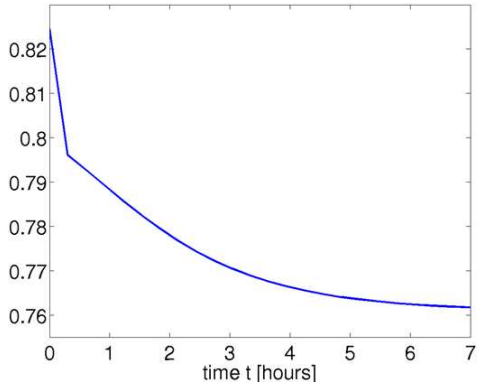

Figure 12: Simulated electric potential Φ_c^S [V]

with $t_0 = 0$ and $t_{M+1} = T$. The free end conditions of the previous optimal control problem are used as prescribed initial conditions for the next optimal control problem.

The numerical results of the optimal control shown in Fig. 13 and 14 are also computed using the software package NUDOCCCS. In Fig. 13 the electric potential in the simulated and the (sub)optimal case are compared. The (sub)optimal cell voltage decreases substantially faster and approaches thereby also faster the new level of voltage under the new cell current. Already in the first optimization interval a good approximation of the stationary value of the cell voltage is reached.

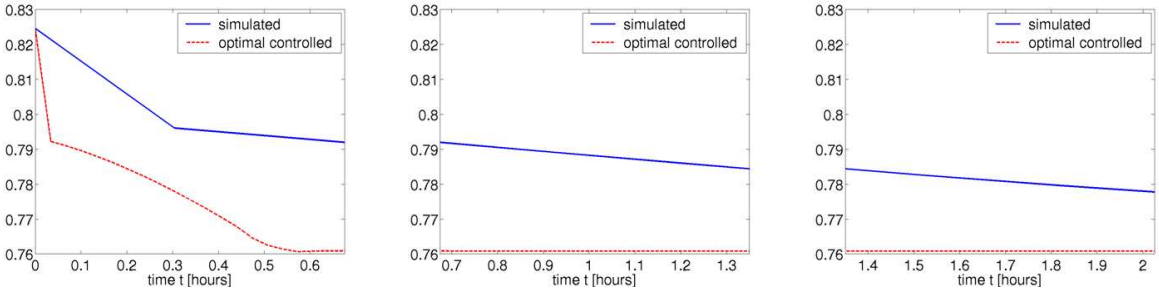

Figure 13: Simulated and (sub)optimal controlled electric potential Φ_c^S [V]

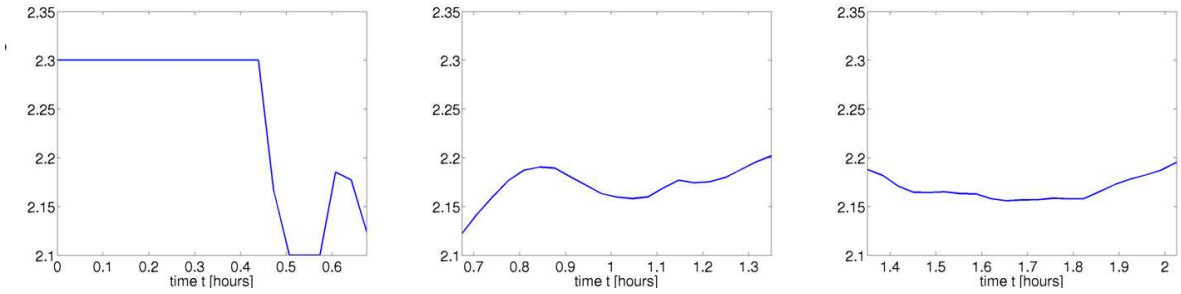

Figure 14: Suboptimal control molar flow density $\gamma_{a,\text{in}}$

Conclusions

A complicated mathematical model, describing the dynamical behavior of a molten carbonate fuel cell, has been presented. The semi-discretization in space of the large scale partial differential algebraic equation

system with integral terms in the right hand side together with its nonstandard boundary conditions including an ODE system yields a very large scale DAE system. The PDAE and the DAE model(s) have index one, so good approximation properties can be expected for the numerical solutions with respect to the exact solutions. The obtained numerical simulation results correspond to the practical experiences of engineers with real fuel cells of the type investigated here. Moreover (sub)optimal boundary controls s.t. to a PDAE were computed for faster load changes of the total cell current.

Acknowledgement. This research is funded by the BMBF within the project *Optimierte Prozessführung von Brennstoffzellensystemen mit Methoden der Nichtlinearen Dynamik.* We are indebted to Prof. Dr.-Ing. K. Sundmacher and Dr.-Ing. P. Heidebrecht for providing us with the complicated fuel cell model and to Prof. Dr. C. Büskens for providing us with his optimal control software NUDOCCCS.

References

[1] Büskens, C., Optimierungsmethoden und Sensitivitätsanalyse für optimale Steuerprozesse mit Steuer- und Zustands-Beschränkungen. Dissertation, Universität Münster, 1998.

[2] Campbell, S.L., Marszalek, W., ODE/DAE integrators and MOL problems. Z. angew. Math. Mech., 76, Suppl. 1 (1996), S 251–S 254.

[3] Campbell, S.L., Marszalek, W., The index of an infinite dimensional implicit system. Math. Comput. Model. Dyn. Syst., 5, 1 (1999), 18–42.

[4] Chudej, K., Heidebrecht, P., Petzet, V., Scherdel, S., Schittkowski, K., Pesch, H.J., Sundmacher, K., Index Analysis and Numerical Solution of a Large Scale Nonlinear PDAE System Describing the Dynamical Behaviour of Molten Carbonate Fuel Cells. Z. angew. Math. Mech., 85, 2 (2005), 132–140.

[5] Günther, M., Wagner, Y., Index concepts for linear mixed systems of differential-algebraic and hyperbolic-type equations. SIAM J. Sci. Comput., 22 (2000), 1610–1629.

[6] Heidebrecht, P., Modelling, Analysis and Optimisation of a Molten Carbonate Fuel Cell with Direct Internal Reforming (DIR-MCFC). VDI Fortschritt Berichte, Reihe 3, Nr. 826, VDI Verlag, Düsseldorf, 2005

[7] Heidebrecht, P., Sundmacher, K., Dynamic Modeling and Simulation of a Countercurrent Molten Carbonate Fuel Cell (MCFC) with Internal Reforming. Fuel Cells, 3–4 (2002), 166–180.

[8] Heidebrecht, P., Sundmacher, K., Molten carbonate fuel cell (MCFC) with internal reforming: model-based analysis of cell dynamics. Chemical Engineering Science, 58 (2003), 1029–1036.

[9] Lamour, R., März, R., Tischendorf, C., PDAEs and Further Mixed Systems as Abstract Differential Algebraic Systems. Preprint 01-11, Institut für Mathematik, Humboldt-Universität zu Berlin, 2001.

[10] Lucht, W., Debrabant, K., On quasi-linear PDAEs with convection: Applications, indices, numerical solution. Appl. Num. Math., 42 (2002), 297–314.

[11] Lucht, W., Strehmel, K., Discretization based indices for semilinear partial differential algebraic equations. Appl. Num. Math., 28 (1998), 371–386.

[12] Lucht, W., Strehmel, K., Eichler-Liebenow, C., Indexes and special discretization methods for linear partial differential algebraic equations. BIT, 39, 3 (1999), 484–512.

[13] Martinson, W.S., Barton, P.I., A differentiation index for partial differential equations. SIAM J. Sci. Comput., 21, 6 (2000), 2295–2315.

[14] Rang, J., Angermann, L., Perturbation index of linear partial differential-algebraic equations. Appl. Num. Math., 53, 2-4 (2005) 437–456.

[15] Rang, J., Chudej, K., A perturbation index for a singular PDE model of a fuel cell. Mathematik-Bericht Nr. 2004/6, Institut für Mathematik, Technische Universität Clausthal, 2004.

[16] Sternberg, K., Simulation, Optimale Steuerung und Sensitivitätsanalyse einer Schmelzcarbonat-Brennstoffzelle. Dissertation, Universität Bayreuth, in preparation.